



Composite exopolysaccharide-based hydrogels extracted from *Nostoc commune* V. as scavengers of soluble methylene blue

Nora Gabriela Herrera^{1,*} , Nelson Adrián Villacrés² ,
Lizbeth Aymara¹ , Viviana Román¹ , Mayra Ramírez¹

¹ Federico Villarreal National University , Lima, Peru

² National University of Engineering , Lima, Peru

* e-mail: nherrera@unfv.edu.pe

Received 26.12.2022; Revised 24.01.2023; Accepted 07.02.2023; Published online 11.07.2023

Abstract:

The industrial water contamination with synthetic dyes is currently a cause for concern. This paper introduces composite hydrogels as alternative scavengers of soluble dyes.

This research used kinetic models and adsorption isotherms to test composite exopolysaccharide hydrogels extracted from *Nostoc commune* V., pectin, and starch for their ability to remove methylene blue from water.

The exopolysaccharides demonstrated a rather low extraction yield and a crystallinity percentage of 38.21%. However, the crystallinity increased in the composite hydrogels (48.95%) with heterogeneous surface. The pseudo-second-order kinetic model served to explain the adsorption mechanism at pH 8 and pH 11, while the Elovich model explained the adsorption mechanism at pH 5. When in acid fluid, the hydrogels had a heterogeneous surface, whereas alkaline fluid resulted in a homogeneous surface. The Temkin adsorption model showed a good fit in the treatments.

At a basic pH value, composite exopolysaccharide-based hydrogels showed good results as scavengers of low-concentration methylene blue.

Keywords: Hydrogel, removal, methylene blue, adsorption, exopolysaccharide, *Nostoc commune* V.

Funding: This research was supported by the Vice-Rectorate for Research of the Federico Villarreal National University (UNFV) as part of The Basic and Applied Research Projects Competition CANON 2019, project No. 5784-2019-CU-UNFV.

Please cite this article in press as: Herrera NG, Villacrés NA, Aymara L, Román V, Ramírez M. Composite exopolysaccharide-based hydrogels extracted from *Nostoc commune* V. as scavengers of soluble methylene blue. *Foods and Raw Materials*. 2024;12(1):37–46. <https://doi.org/10.21603/2308-4057-2024-1-587>

INTRODUCTION

The term *microalgae* refers to both eukaryotic (microalgae) and prokaryotic (cyanobacteria) microorganisms that perform oxygenic photosynthesis. These organisms live in aquatic and terrestrial habitats. They produce various compounds, e.g., polyunsaturated fatty acids, pigments, proteins, some enzymes, and exopolysaccharides. These compounds can be applied in various biotechnology sectors, i.e., food, energy, health, and biomaterials [1, 2].

Cyanobacterial exopolysaccharides possess unique biochemical properties due to their high molecular weight, anionic properties, and acidic profile [3]. Exopolysaccharides extracted from *Nostoc commune* V. can be applied in biomedicine and food industry to produce

hydrogels and films. However, the chemical structure of these exopolysaccharides is not yet known [3, 4].

Hydrogels consist of three-dimensional networks of intertwined polymer chains that are able to absorb and retain water molecules and solutes, including such ionic dyes as methylene blue [5].

Methylene blue is a cationic thiazine dye used in textile industries. However, it affects human health by causing asthma, cancer, and mutations [6]. Moreover, it affects the growth of aquatic organisms and generates mutagenic effects in fish [7, 8].

Industrial development facilitates economic prosperity but causes water pollution [9, 10]. This type of pollution occurs because various industries that deal with textile, dyes, and pharmaceuticals discharge

effluents that usually contain dyes and/or heavy metals [11]. For example, more than 700 000 tons of dyes are produced annually, of which approximately 1–2% are drained during production and around 10–15% are eliminated as effluents during application [12].

The list of modern wastewater treatment methods includes chemical precipitation, filtration, reverse osmosis, and photo-degradation [13–16]. However, not only are all these methods expensive and complex, but they also generate secondary products [17].

As a result, scientists are on the look for new absorbents, such as hydrogels, that could remove contaminants, e.g., dyes, from wastewater [18, 19].

This research extracted exopolysaccharides from the *N. commune* to prepare a new composite hydrogel that would remove soluble methylene blue.

STUDY OBJECTS AND METHODS

Materials. Pectin, starch, and calcium chloride dihydrate were purchased from Sigma-Aldrich. Petroleum ether, chloroform, propanol, ethanol, and methylene blue were obtained from Merck. The exopolysaccharides were extracted from cyanobacteria *Nostoc commune* V. collected in Conococha Lake, Province of Bolognesi, Ancash-Peru. These cyanobacteria were dried, crushed, and stored in an amber jar at room temperature.

Extracting the exopolysaccharide. We defatted 2 g of dry powder by maceration with 100 mL of petroleum ether, followed by filtering and oven-drying. This process was repeated with chloroform and then with ethanol. The extraction of the exopolysaccharide followed the procedure described by Rodríguez *et al.* [20]. The extractant was precipitated with propanol for subsequent drying, grinding, and storage in an amber bottle. The exopolysaccharide yield (Y_e , %) was calculated as follows:

$$Y_e = \frac{W_1}{W_2} \times 100 \quad (1)$$

where W_1 is the weight of exopolysaccharide, g; and W_2 is the weight of *N. commune* dried powder, g.

Preparation of hydrogels. We diluted 0.05 g of exopolysaccharide in distilled water to mix it with a pectin-starch solution in a ratio of 2:0.5, according to the methodology described by Dafe *et al.* [21]. After that, we poured the resulting mix drop by drop into a 0.2 M solution of $\text{CaCl}_2 \cdot 2\text{H}_2\text{O}$ under constant stirring at room temperature. The hydrogels were filtered and washed with distilled water. Before each application, the hydrogels were dried at 30°C for 36 h until a constant weight was obtained.

Characterization. The FTIR-ATR spectra (600 to 4000 cm^{-1}) were obtained using a Nicolet iS10 Thermo Scientific spectrophotometer. The thermogravimetric curves were gathered in an STA 6000 PerkinElmer device using 5.0 ± 0.1 mg of the sample in an N_2 atmosphere. The flow rate was 20 mL/min, and the temperature was between 20 and 600°C with a heating rate of 10°C/min. The XRD diffractograms were obtained

using a D2 Phaser (Brüker) equipment in a range of 10° to 60°. The crystallinity (%) index was determined using the ratio between the crystalline area and the total area (Eq. (2)). The specific surface area was determined using a Gemini VII 2390t micrometer with the nitrogen adsorption and desorption technique. The SEM images were obtained with an FEI Inspect S50 microscope. The samples were gold-plated in an 11430E-AX (SPI Supplies) high vacuum metallizer:

$$\text{Crystallinity} = \frac{\text{Crystalline area}}{\text{Total area}} \times 100 \quad (2)$$

Removing methylene blue. We added 0.1 g of hydrogel to 50 mL of methylene blue solution. For isothermal studies, the methylene blue concentration was $1.0\text{--}1.5 \times 10^{-6}$ mol/L at 25°C. The experiment involved five-time intervals (15, 30, 60, 90, and 120 min) and three pH levels (5, 8, and 11). The pH values were adjusted with NaOH (0.1 mol/L) and HCl (0.1 mol/L). The absorbance values ($\lambda_{\text{max}} = 668$ nm) were obtained using a Thermo Scientific/Spectronic GENESYS 20 Visible spectrophotometer by quantifying the adsorption capacity (q_e , mg/g) and removal percentage (%):

$$q_e = \frac{V \times (C_0 - C_e)}{W} \quad (3)$$

$$\text{Removal} = \frac{C_0 - C_e}{C_0} \times 100 \quad (4)$$

where C_0 and C_e are the initial and V equilibrium concentrations of methylene blue, mg/L, respectively; W is the volume of the solution, L; W is the mass of the hydrogel, g.

Isotherm and kinetic models. The adsorption isotherm illustrates the mobility or retention of a substance using a solid phase at a constant pH and temperature. The Langmuir isotherm (Eq. (5)) is an empirical model that describes the adsorption process on a homogeneous surface, forming a single layer without lateral interaction between the absorbed molecules. On the contrary, the Freundlich isotherm (Eq. (6)) assumes that the adsorption is carried out on a heterogeneous surface via a multilayer process, while the Temkin isotherm (Eq. (7)) considers the interaction between the adsorbent and the adsorbate:

$$\frac{C_e}{q_e} = \frac{1}{K_L \times q_{\text{max}}} + \frac{C_e}{q_{\text{max}}} \quad (5)$$

$$\ln q_e = \ln b + \frac{1}{n} \ln C_e \quad (6)$$

$$q_e = \frac{RT}{b_T} \ln C_e + \frac{RT}{b} \ln k_m \quad (7)$$

where C_e is the adsorbate equilibrium concentration, mg/L; q_e is the adsorbed amount at equilibrium, mg/g; q_{max} is the maximal amount of adsorbed surfactant, mg/g; K_L is the Langmuir constant, L/mg; b is the adsorption

capacity, L/mg; $1/n$ is the adsorption intensity or surface heterogeneity; R is the universal gas constant, J/mol/K; T is the temperature, K; b_T is the Temkin constant related to sorption heat, J/mol; k_m is the Temkin isotherm constant, L/g.

Finally, the separation factor or equilibrium parameter (Eq. (8)), denoted as R_L , checks if the adsorption is favorable ($R_L < 1$) or unfavorable ($R_L > 1$):

$$R_L = \frac{1}{1 + K_L \times C_0} \quad (8)$$

The pseudo-first-order (Eq. (9)) and pseudo-second-order (Eq. (10)) kinetic models differentiated the kinetic equations according to the adsorption capacity affected by the initial concentration of the dye. The Elovich model (Eq. (11)) assumes that the adsorbent surfaces are heterogeneous, and adsorption is performed in a multilayer process:

$$\ln \left[1 - \frac{q_t}{q_e} \right] = -k_1 \times t \quad (9)$$

$$\frac{1}{q_e - q_t} - \frac{1}{q_e} = k_2 \times t \quad (10)$$

$$q_t = \left(\frac{1}{\beta} \right) \times \ln \left(\frac{\alpha}{\beta} \right) + \left(\frac{1}{\beta} \right) \times \ln t \quad (11)$$

where q_e is the amount of the adsorbate at equilibrium, mg/g; q_t is the maximal uptake of adsorbate, mg/g; k_1 is the pseudo-first-order rate constant; k_2 is the pseudo-second-order rate constant; t is the contact time with

adsorbent, min; α is initial sorption rate, mg/g/min; β is the extent of surface coverage and activation energy for chemisorption, g/mg [22, 23].

RESULTS AND DISCUSSION

Exopolysaccharide profile. The exopolysaccharide obtained from the *Nostoc commune* V. had a brown-amber color (Fig. 1a); the extraction yield was 25% dw. However, Wang *et al.* managed to obtain a much greater yield of 96.7% [24].

X-ray analysis. The X-ray diffractogram (Fig. 1b) showed a broad peak at 20° and a bun-shaped curve, which suggested the non-crystallinity of the exopolysaccharides extracted from cyanobacteria [20]. This result was found consistent because the exopolysaccharide had crystallinity of 38.21% (Fig. 2b).

Thermogravimetry of exopolysaccharides. Figure 1c presents the TG thermogravimetric curve of the exopolysaccharide with mass losses assigned to the following thermal events: dehydration, depolymerization, degradation, and carbonization [20]. Table 1 shows the percentage of mass loss in each thermal event, with their respective temperature intervals.

FTIR of exopolysaccharides. Figure 1d illustrates the FTIR spectrum of the exopolysaccharide sample. The spectrum showed signals at 3325 cm^{-1} (hydroxyl groups), 2923 cm^{-1} (C-H vibrational stretch), 1586 cm^{-1} (asymmetric stretching of $-\text{COO}^-$), 1416 cm^{-1} (symmetric stretching of $-\text{COO}^-$), 1019 cm^{-1} (C-O-C vibrational stretch in cyclic glucose units), 889 cm^{-1} (β -glycosidic bond), and 795 cm^{-1} (glucopyranose units) [3, 25].

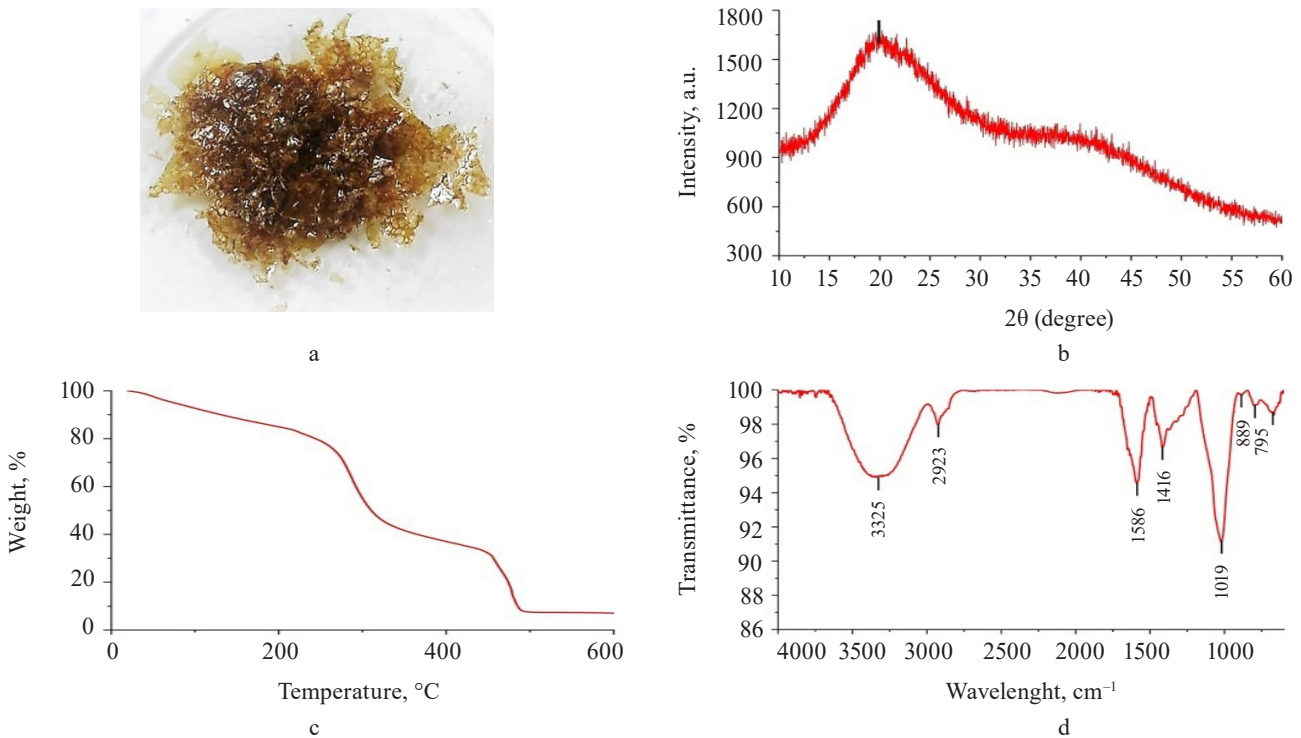


Figure 1 Extracted sample (a); XRD diffractogram (b); TG curve (c); and FTIR spectrum (d) of exopolysaccharide from *Nostoc commune*

Table 1 Mass loss values: thermogravimetric analysis of exopolysaccharide obtained from *Nostoc commune*

Weight, mg	Thermal event	ΔT , °C	Mass loss, %
4.965	Dehydration	20.0–186.0	14.1
	Depolymerization	186.0–413.0	49.9
	Degradation	413.0–558.0	28.8
	Carbonization	558.0–600.0	2.8

Table 2 Mass loss values: thermogravimetric analysis of exopolysaccharide-based composite hydrogels

Weight, mg	Thermal event	ΔT , °C	Mass loss, %
5.297	Dehydration	30.0–150.0	1.5
	Degradation	150.0–440.5	88.9
	Carbonization	440.5–600.0	3.3

Exopolysaccharide-based composite hydrogel profile. Exopolysaccharide-based composite hydrogels had crystallinity of 48.95% (Fig. 2a). The XRD diffractogram (Fig. 2b) showed peaks close to 15 and 22°, which corresponded to the gelatinized starch chains [26]. On the other hand, a peak around 34° corresponded to the crystalline structure of pectin [27]. However, the broad peak at 20°, which corresponded to the exopolysaccharides, disappeared, probably because the exopolysaccharide structure was destroyed.

Figure 2c presents the TG thermogravimetric curve of compound hydrogels with mass losses assigned to the stages of dehydration, degradation, and carbonization. According to Dash *et al.*, the second stage consists of

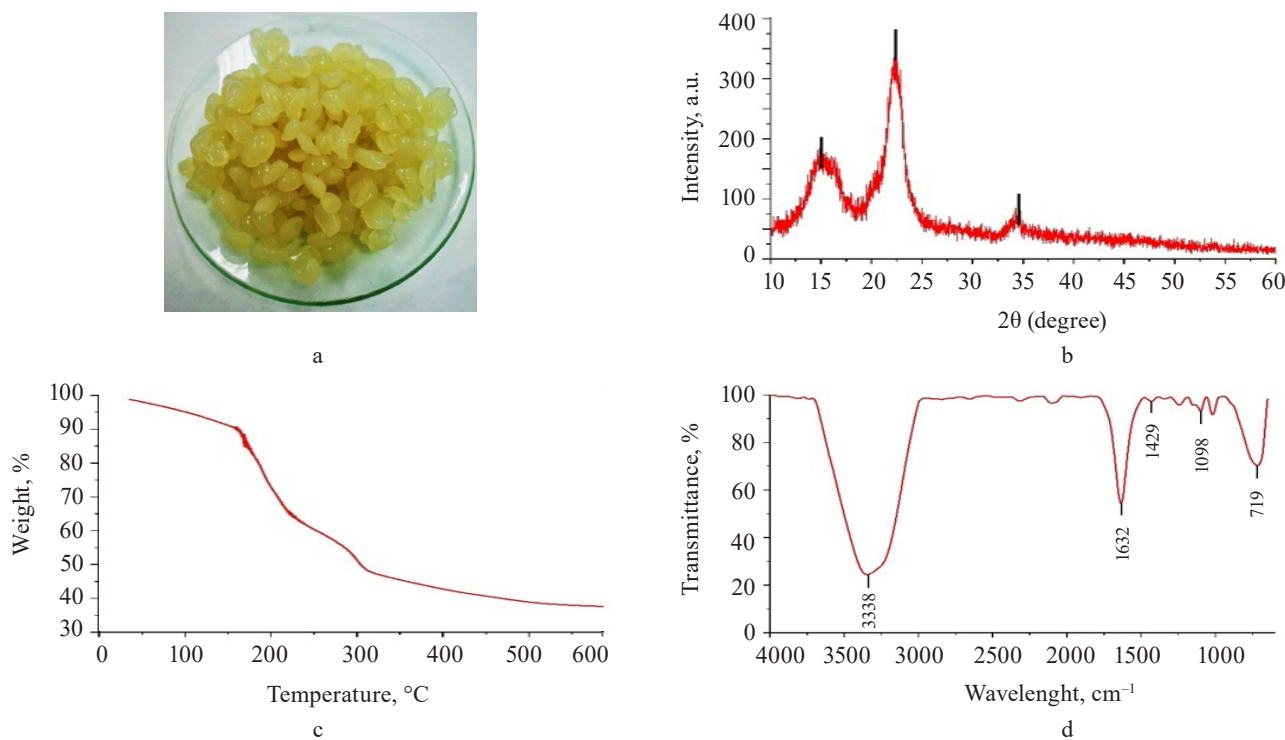
two continuous processes that follow pectin (200–280°C) and starch (290–425°C) degradation [28]. Table 2 shows the percentage of mass loss in each thermal event with their respective temperature intervals.

The FTIR spectrum of the hydrogels (Fig. 2d) shows additional signals to the spectrum of the exopolysaccharide (Fig. 1d). These signals corresponded to the C=O carbonyl group (1632 cm^{-1}) for pectin, while the peaks at 1429 and 1098 cm^{-1} could be attributed to C-O-O stretching and C-O-H bending modes in starch, respectively, and the signal at 719 cm^{-1} could be correlated with vibrations belonging of the polysaccharide ring [29–31].

The specific surface area of the composite hydrogel, as obtained from the BET isotherm model, was 0.5616 m^2/g . Figure 3 shows the N_2 adsorption-desorption process of the hydrogel before methylene blue scavenging. This process was a type VI isotherm, which is typical of solids with a uniform non-porous surface and represents a multilayer adsorption [31].

After the removal process, the composite hydrogels turned blue (Fig. 4a). Figure 4b shows a decrease in the band at 1632 cm^{-1} . However, the increase in pH to basic levels intensified the bands: at pH 11, the removal process probably occurred by electrostatic attraction [32, 33].

The SEM images of the hydrogels revealed the superficial changes in these materials during the methylene blue scavenging at different pH values. At pH 5 (Fig. 5b), the surface of the hydrogel became smoother and more homogeneous, compared to the hydrogel

**Figure 2** Samples (a); XRD diffractogram (b); TG curve (c); and FTIR spectrum (d) of exopolysaccharide-based composite hydrogel

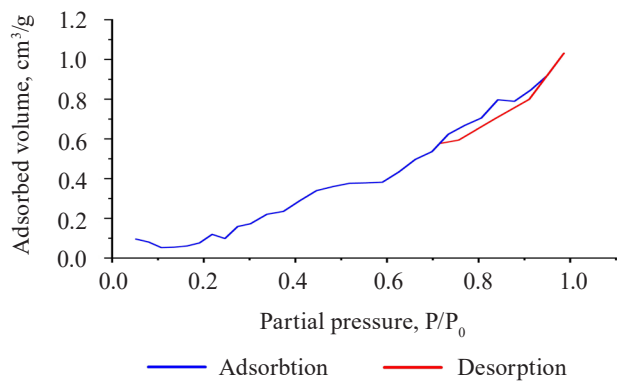


Figure 3 BET sorption-desorption isotherms for the exopolysaccharide-based composite hydrogel

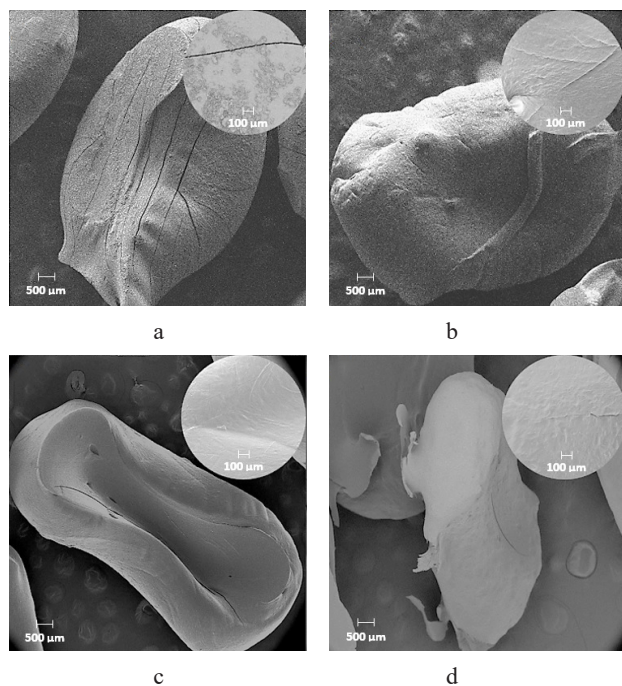


Figure 5 SEM images of hydrogels before (a) and after methylene blue removal at pH 5 (b), pH 8 (c), and pH 11 (d)

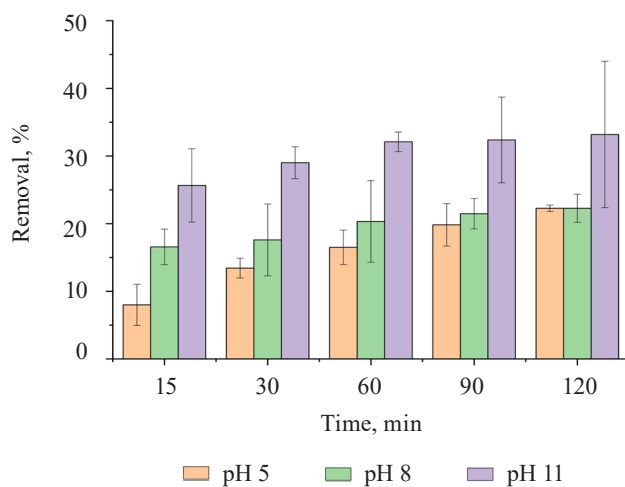


Figure 6 Methylene blue removal percentages at different pH and time values

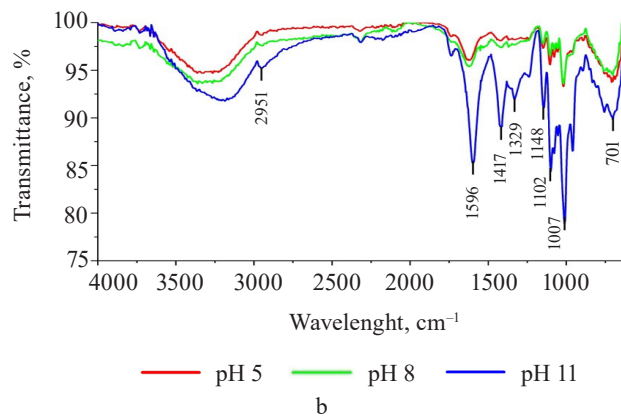
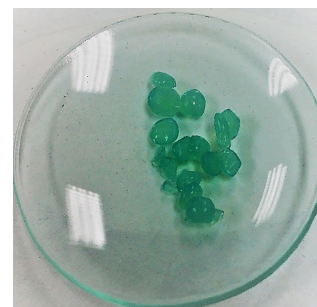


Figure 4 Samples (a) and FTIR spectrum (b) of exopolysaccharide-based composite hydrogel after methylene blue removal

before scavenging (Fig. 5a). At pH 8 (Fig. 5c), the hydrogel improved its surface homogeneity but changed shape. The same pattern occurred at pH 11 (Fig. 5d).

Methylene blue percentage removal. Figure 6 shows an increase in methylene blue scavenging at a basic pH value (pH 11) for 120 min. The increase could be explained by the more negative charge on the adsorbent surface, which generated a greater electrostatic attraction with the positively charged adsorbate [34]. Table 3 summarizes the methylene blue removal percentages at different pH levels and processing times.

Kinetic adsorption models. The pseudo-first-order, pseudo-second-order, and Elovich kinetic models were used to verify the experimental data (Fig. 7). Table 4 shows the values of the constants for the different kinetic models.

The pseudo-second-order model showed a higher R^2 value in the scavenging processes at pH 8 and pH 11. On the other hand, the Elovich model demonstrated a higher value at pH 5. Apparently, the mechanism of methylene blue sorption at pH 8 and pH 11 was caused by chemisorption. At pH 5, the surface of the hydrogel was heterogeneous, which was in line with Fig. 5b [35].

Adsorption isotherm models. We employed the Langmuir, Freundlich, and Temkin isotherms to verify the experimental data (Fig. 8). Table 5 shows the values that correspond to the adsorption isotherm models.

Negative R_L values were obtained from methylene blue removal at different pH values. At the three

Table 3 Methylene blue percentage removal and adsorption capacity

Time, min	pH	Initial methylene blue concentration, mg/L	Adsorption capacity, mg/g	Methylene blue removal, %
15	5	1.045×10^{-6}	4.669×10^{-7}	8.00
	8	1.014×10^{-6}	4.070×10^{-7}	16.57
	11	1.019×10^{-6}	3.623×10^{-7}	25.66
30	5	1.151×10^{-6}	4.817×10^{-7}	13.44
	8	1.117×10^{-6}	4.520×10^{-7}	17.59
	11	1.146×10^{-6}	4.067×10^{-7}	29.02
60	5	1.275×10^{-6}	5.054×10^{-7}	16.50
	8	1.209×10^{-6}	4.698×10^{-7}	20.34
	11	1.226×10^{-6}	4.231×10^{-7}	32.11
90	5	1.394×10^{-6}	5.587×10^{-7}	19.83
	8	1.286×10^{-6}	5.131×10^{-7}	21.48
	11	1.358×10^{-6}	4.936×10^{-7}	32.38
120	5	1.459×10^{-6}	6.054×10^{-7}	22.28
	8	1.429×10^{-6}	5.917×10^{-7}	22.28
	11	1.469×10^{-6}	5.503×10^{-7}	33.18

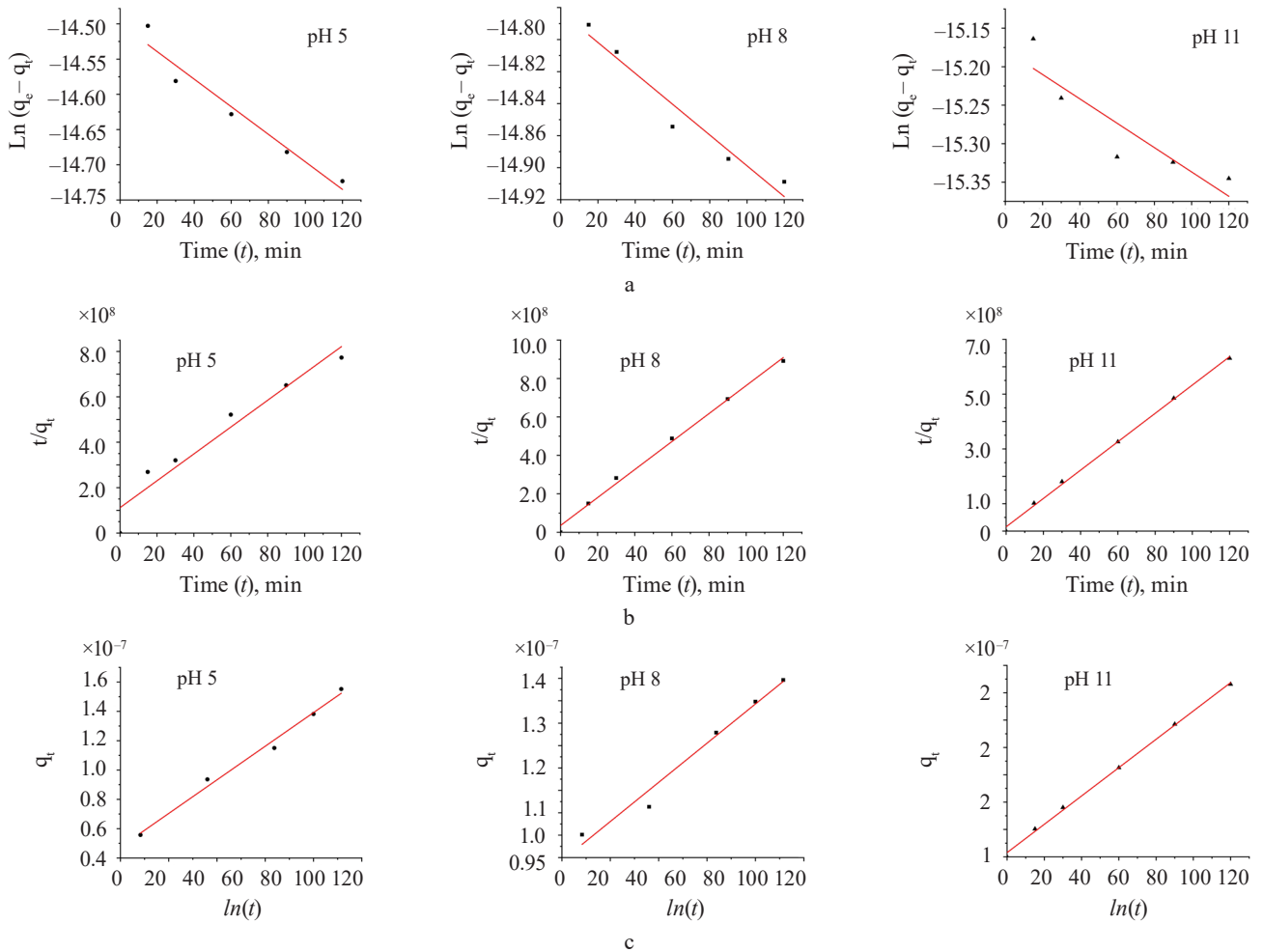


Figure 7 Linear plots for methylene blue adsorption: pseudo-first-order model (a); pseudo-second-order model (b); and Elovich kinetic model (c)

pH levels, the methylene blue removal did not fit the Langmuir isotherm [36, 37]. However, the adsorption intensity ($1/n$) in all the treatments was below one, which suggested that the active centers had less and less free enthalpy [38]. The b_T values were negative, so

the adsorption process in all the treatments were endothermic [39]. The results indicated a good fit (R^2) with the Temkin model; therefore, this model explained the adsorption process between the adsorbate and the adsorbent.

Table 4 Parameter values of methylene blue removal: kinetic studies

pH value	Kinetic model	R^2	K_1	K_2	α , mg/g/min	β , g/mg
pH 5	Pseudo-first-order	0.9331	-1.633×10^{-5}	/	/	/
	Pseudo-second-order	0.9257	/	3.120×10^5	/	/
	Elovich	0.9857	/	/	2.180×10^7	1.059×10^{-8}
pH 8	Pseudo-first-order	0.9324	-8.017×10^{-6}	/	/	/
	Pseudo-second-order	0.9942	/	1.516×10^6	/	/
	Elovich	0.9708	/	/	5.715×10^7	3.147×10^{-7}
pH 11	Pseudo-first-order	0.7549	-1.317×10^{-5}	/	/	/
	Pseudo-second-order	0.9980	/	1.724×10^6	/	/
	Elovich	0.9464	/	/	4.824×10^7	1.911×10^{-6}

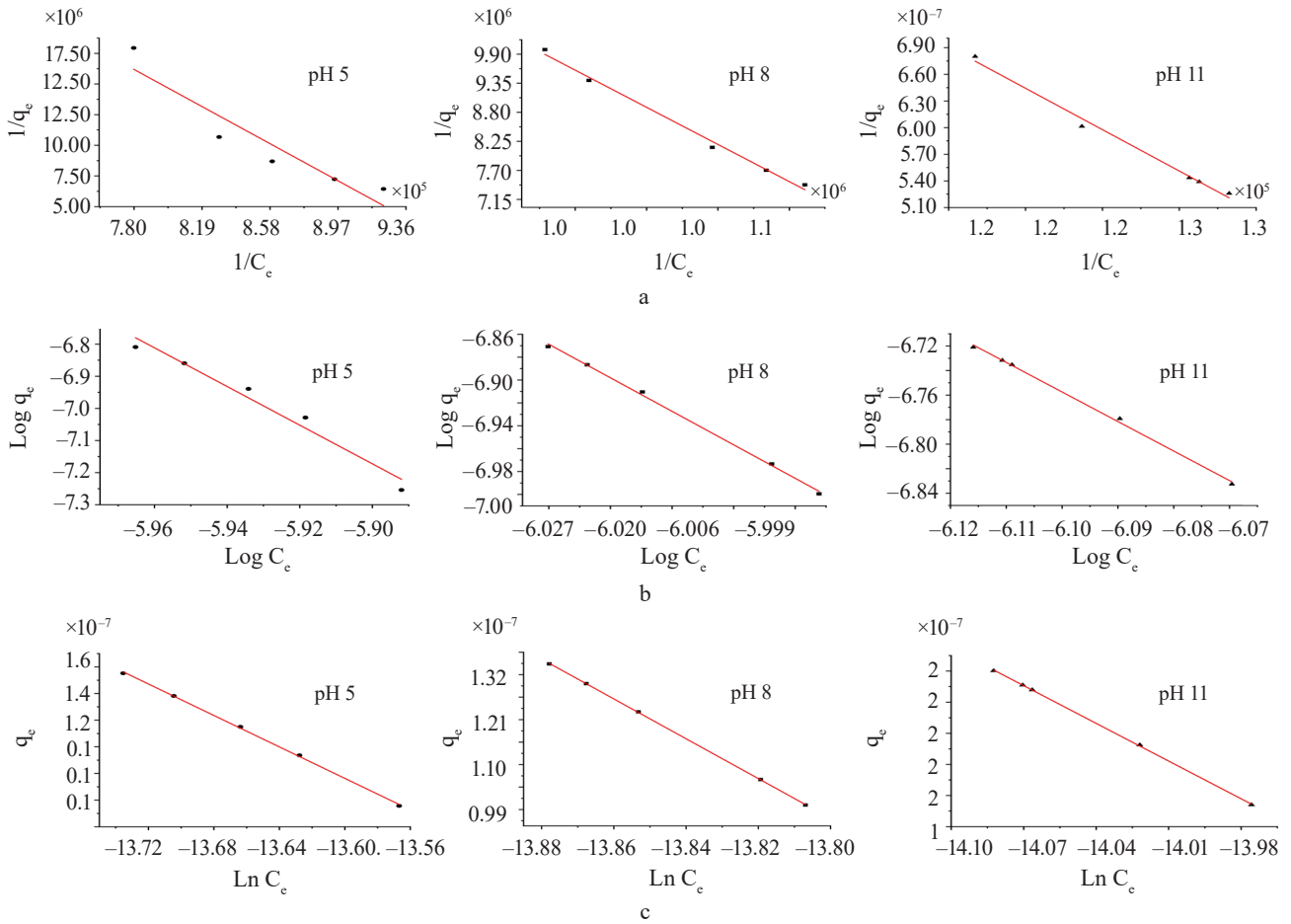


Figure 8 Linear plots for methylene blue adsorption: Langmuir model (a); Freundlich model (b); and Temkin model (c)

Table 5 Parameter values of methylene blue removal: adsorption studies

Type of isotherm	Parameters	Methylene blue removal		
		pH 5	pH 8	pH 11
Langmuir	K_L , L/mg	-9.89×10^5	-1.273×10^6	-1.753×10^6
	q_{max} , mg/g	1.30×10^{-8}	2.234×10^{-8}	4.898×10^{-8}
	R_L	-2.65	-1.86	-0.99
	R^2	0.8495	0.9912	0.9893
Freundlich	K_F , mg/g	2.09×10^{-43}	8.30×10^{-33}	3.51×10^{-22}
	$1/n$	-6.02	-4.18	-2.41
	R^2	0.9587	0.9978	0.9973
Temkin	K_m , L/g	7.08×10^5	8.07×10^5	8.15×10^5
	b_T , J/mol	-5.901×10^{-7}	-4.871×10^{-7}	-4.04×10^{-7}
	R^2	0.9991	0.9999	0.9997

CONCLUSION

Exopolysaccharides from *Nostoc commune* V. yielded composite hydrogels that could act as methylene blue scavengers. These materials had a non-porous and heterogeneous surface, which underwent changes at basic pH values during the removal process. The methylene blue adsorption mechanism depended on chemisorption and endothermic processes. The maximal removal was 33.18%, which proved that these composite hydrogels were not efficient as methylene blue scavengers. The result open pros-

pects for further research of exopolysaccharides with other adsorption materials.

CONTRIBUTION

The authors were equally involved in writing the manuscript and are equally responsible for any potential plagiarism.

CONFLICT OF INTEREST

The authors declare no conflict of interests regarding the publication of this article.

REFERENCES

1. Laroche C. Exopolysaccharides from microalgae and cyanobacteria: Diversity of strains, production strategies, and applications. *Marine Drugs*. 2022;20(5). <https://doi.org/10.3390/md20050336>
2. Miguel SP, Ribeiro MP, Otero A, Coutinho P. Application of microalgae and microalgal bioactive compounds in skin regeneration. *Algal Research*. 2021;58. <https://doi.org/10.1016/j.algal.2021.102395>
3. Montero X, Alves A, Ribeiro MP, Lazari M, Coutinho P, Otero A. Biochemical characterization of *Nostoc* sp. exopolysaccharides and evaluation of potential use in wound healing. *Carbohydrate Polymers*. 2021;254. <https://doi.org/10.1016/j.carbpol.2020.117303>
4. Gonzales KN, Troncoso OP, Torres FG, López D. Molecular α -relaxation process of exopolysaccharides extracted from *Nostoc commune* cyanobacteria. *International Journal of Biological Macromolecules*. 2020;161:1516–1525. <https://doi.org/10.1016/j.ijbiomac.2020.07.268>
5. Paulino AT, Guilherme MR, Reis AV, Campese GM, Muniz EC, Nozaki J. Removal of methylene blue dye from an aqueous media using superabsorbent hydrogel supported on modified polysaccharide. *Journal of Colloid and Interface Science*. 2006;301(1):55–62. <https://doi.org/10.1016/j.jcis.2006.04.036>
6. Shah SS, Ramos B, Teixeira ACSC. Adsorptive removal of methylene blue dye using biodegradable superabsorbent hydrogel polymer composite incorporated with activated charcoal. *Water*. 2022;14(20). <https://doi.org/10.3390/w14203313>
7. Varghese SA, Rangappa SM, Siengchin S, Parameswaranpillai J. Natural polymers and the hydrogels prepared from them. In: Chen Y, editor. *Hydrogels based on natural polymers*. Elsevier; 2020. pp. 17–47. <https://doi.org/10.1016/b978-0-12-816421-1.00002-1>
8. Shooto ND, Nkutha CS, Guilande NR, Naidoo EB. Pristine and modified mucuna beans adsorptive studies of toxic lead ions and methylene blue dye from aqueous solution. *South African Journal of Chemical Engineering*. 2020;31:33–43. <https://doi.org/10.1016/j.sajce.2019.12.001>
9. Hong G-B, Yu T-J, Lee H-C, Ma C-M. Using rice bran hydrogel beads to remove dye from aqueous solutions. *Sustainability*. 2021;13(10). <https://doi.org/10.3390/su13105640>
10. Drozdova MYu, Pozdnyakova AV, Osintseva MA, Burova NV, Minina VI. The microorganism-plant system for remediation of soil exposed to coal mining. *Foods and Raw Materials*. 2021;9(2):406–418. <https://doi.org/10.21603/2308-4057-2021-2-406-418>
11. Ren J, Wang X, Zhao L, Li M, Yang W. Effective removal of dyes from aqueous solutions by a gelatin hydrogel. *Journal of Polymers and the Environment*. 2021;29:3497–3508. <https://doi.org/10.1007/s10924-021-02136-z>
12. Hussain S, Khan N, Gul S, Khan S, Khan H. Contamination of water resources by food dyes and its removal technologies. In: Eyvaz M, Yüksel E, editors. *Water chemistry*. IntechOpen; 2019. <https://doi.org/10.5772/intechopen.90331>
13. Sane PK, Tambat S, Sontakke S, Nemade P. Visible light removal of reactive dyes using CeO₂ synthesized by precipitation. *Journal of Environmental Chemical Engineering*. 2018;6(4):4476–4489. <https://doi.org/10.1016/j.jece.2018.06.046>
14. Mansor ES, Ali H, Abdel-Karim A. Efficient and reusable polyethylene oxide/polyaniline composite membrane for dye adsorption and filtration. *Colloid and Interface Science Communications*. 2020;39. <https://doi.org/10.1016/j.colcom.2020.100314>
15. Wang J, Zhang T, Mei Y, Pan B. Treatment of reverse-osmosis concentrate of printing and dyeing wastewater by electro-oxidation process with controlled oxidation-reduction potential (ORP). *Chemosphere*. 2018;201:621–626. <https://doi.org/10.1016/j.chemosphere.2018.03.051>

16. Nayak S, Prasad SR, Mandal D, Das P. Carbon dot cross-linked polyvinylpyrrolidone hybrid hydrogel for simultaneous dye adsorption, photodegradation and bacterial elimination from waste water. *Journal of Hazardous Materials*. 2020;392. <https://doi.org/10.1016/j.jhazmat.2020.122287>
17. Ammari Y, El Atmani K, Bay L, Bakas I, Qourzal S, Ait Ichou I. Elimination of a mixture of two dyes by photocatalytic degradation based on TiO₂ P-25 Degussa. *Materials Today: Proceedings*. 2020;22:126–129. <https://doi.org/10.1016/j.matpr.2019.08.142>
18. ALSamman MT, Sánchez J. Recent advances on hydrogels based on chitosan and alginate for the adsorption of dyes and metal ions from water. *Arabian Journal of Chemistry*. 2021;14(12). <https://doi.org/10.1016/j.arabjc.2021.103455>
19. Elhady MA, Mousaa IM, Attia RM. Preparation of a novel superabsorbent hydrogel based on polyacrylic acid/shellac using gamma irradiation for adsorption removal of malachite green dye. *Polymers and Polymer Composites*. 2022;30. <https://doi.org/10.1177/09673911221074435>
20. Rodriguez S, Torres FG, López D. Preparation and characterization of polysaccharide films from the cyanobacteria *Nostoc commune*. *Polymers from Renewable Resources*. 2017;8(4):133–150. <https://doi.org/10.1177/204124791700800401>
21. Dafe A, Etemadi H, Dilmaghani A, Mahdavinia GR. Investigation of pectin/starch hydrogel as a carrier for oral delivery of probiotic bacteria. *International Journal of Biological Macromolecules*. 2017;97:536–543. <https://doi.org/10.1016/j.ijbiomac.2017.01.060>
22. Hii HT. Adsorption isotherm and kinetic models for removal of methyl orange and Remazol brilliant blue R by coconut shell activated carbon. *Tropical Aquatic and Soil Pollution*. 2021;1(1):1–10. <https://doi.org/10.53623/tasp.v1i1.4>
23. Kalam S, Abu-Khamsin SA, Kamal MS, Patil S. Surfactant adsorption isotherms: A review. *ACS Omega*. 2021;6(48):32342–32348. <https://doi.org/10.1021/acsomega.1c04661>
24. Wang H-B, Wu S-J, Liu D. Preparation of polysaccharides from cyanobacteria *Nostoc commune* and their antioxidant activities. *Carbohydrate Polymers*. 2014;99:553–555. <https://doi.org/10.1016/j.carbpol.2013.08.066>
25. Dubessay P, Andhare P, Kavitate D, Shetty PH, Ursu AV, Delattre C, et al. Microbial glucuronans and succinoglycans. In: Oliveira JM, Radhouani H, Reis RL, editors. *Polysaccharides of microbial origin*. Cham: Springer; 2021. pp. 1–23. https://doi.org/10.1007/978-3-030-35734-4_8-1
26. Abd El-Ghany NA, Mahmoud ZM. Synthesis, characterization and swelling behavior of high-performance antimicrobial amphoteric hydrogels from corn starch. *Polymer Bulletin*. 2020;78(1):6161–6182. <https://doi.org/10.1007/s00289-020-03417-8>
27. Sani IK, Geshlaghi SP, Pirsas S, Asdagh A. Composite film based on potato starch/apple peel pectin/ZrO₂ nanoparticles/microencapsulated *Zataria multiflora* essential oil; investigation of physicochemical properties and use in quail meat packaging. *Food Hydrocolloids*. 2021;117. <https://doi.org/10.1016/j.foodhyd.2021.106719>
28. Dash KK, Ali NA, Das D, Mohanta D. Thorough evaluation of sweet potato starch and lemon-waste pectin based-edible films with nano-titania inclusions for food packaging applications. *International Journal of Biological Macromolecules*. 2019;139:449–458. <https://doi.org/10.1016/j.ijbiomac.2019.07.193>
29. Nsom MV, Etape EP, Tendo JF, Namond BV, Chongwain PT, Yufanyi MD, et al. A green and facile approach for synthesis of starch-pectin magnetite nanoparticles and application by removal of methylene blue from textile effluent. *Journal of Nanomaterials*. 2019;2019. <https://doi.org/10.1155/2019/4576135>
30. Guo X, Duan H, Wang C, Huang X. Characteristics of two calcium pectinates prepared from citrus pectin using either calcium chloride or calcium hydroxide. *Journal of Agricultural and Food Chemistry*. 2014;62(27):6354–6361. <https://doi.org/10.1021/jf5004545>
31. Sing KSW, Everett DH, Haul RAW, Moscou L, Pierotti RA, Rouquérol J, et al. Reporting physisorption data for gas/solid systems with special reference to the determination of surface area and porosity (Recommendations 1984). *Pure and Applied Chemistry*. 1985;57(4):603–619. <https://doi.org/10.1351/pac198557040603>
32. Veisi Z, Gallant ND, Alcantar NA, Toomey RG. Responsive coatings from naturally occurring pectin polysaccharides. *Colloids and Surfaces B: Biointerfaces*. 2019;176:387–393. <https://doi.org/10.1016/j.colsurfb.2018.12.060>
33. Arayaphan J, Maijan P, Boonsuk P, Chantarak S. Synthesis of photodegradable cassava starch-based double network hydrogel with high mechanical stability for effective removal of methylene blue. *International Journal of Biological Macromolecules*. 2021;168:875–886. <https://doi.org/10.1016/j.ijbiomac.2020.11.166>
34. Pathania D, Sharma S, Singh P. Removal of methylene blue by adsorption onto activated carbon developed from *Ficus carica* bast. *Arabian Journal of Chemistry*. 2017;10:S1445–S1451. <https://doi.org/10.1016/j.arabjc.2013.04.021>
35. Sahoo TR, Prelot B. Adsorption processes for the removal of contaminants from wastewater. In: Bonelli B, Freyria FS, Rossetti I, Sethi R, editors. *Nanomaterials for the detection and removal of wastewater pollutants. A volume in micro and nano technologies*. Elsevier; 2020. pp. 161–222. <https://doi.org/10.1016/B978-0-12-818489-9.00007-4>

36. Linde MP, Marquez K. Alkali lignin from rice (*Oryza sativa* L.) husk as adsorbent for aqueous methyl orange and bromothymol blue: Analysis of the adsorption kinetics and mechanism. *Kimika*. 2021;32(1):19–33. <https://doi.org/10.26534/kimika.v32i1.19-33>
37. Asaolu SS, Adefemi SO, Ibigbami OA, Adekeye DK, Olagboye SA. Kinetics, isotherm and thermodynamic properties of the basement complex of clay deposit in Ire-Ekiti southwestern Nigeria for heavy metals removal. *Nature Environment and Pollution Technology an International Quarterly Scientific Journal*. 2020;19(3):897–907. <https://doi.org/10.46488/NEPT.2020.v19i03.001>
38. Ronka S, Bodylska W. Sorption properties of specific polymeric microspheres towards desethyl-terbuthylazine and 2-hydroxy-terbuthylazine: Batch and column studies. *Materials*. 2021;14(11). <https://doi.org/10.3390/ma14112734>
39. Fathy NA, El-Shafey OI, Khalil LB. Effectiveness of alkali-acid treatment in enhancement the adsorption capacity for rice straw: The removal of methylene blue dye. *ISRN Physical Chemistry*. 2013;2013. <https://doi.org/10.1155/2013/208087>

ORCID IDs

Nora Gabriela Herrera  <https://orcid.org/0000-0003-0595-8747>

Nelson Adrián Villacrés  <https://orcid.org/0000-0001-9499-3792>

Lizbeth Aymara  <https://orcid.org/0000-0001-9358-7688>

Viviana Román  <https://orcid.org/0000-0002-6614-3632>

Mayra Ramírez  <https://orcid.org/0000-0002-9143-4060>